Inorganic Chemistry
Article
Cite This: Inorg. Chem. 2019, 58, 3435−3443
pubs.acs.org/IC

Layered Compounds BaFMgPn (Pn = P, As, Sb, and Bi), Transition-Metal-Free Representatives of the 1111 Structure Type

Igor V. Plokhikh,*[,†] Alexey N. Kuznetsov,[§,⊥] Dmitri O. Charkin,[§] Andrei V. Shevelkov,[§] and Arno Pfitzner*[,†]

[†]Univeristy of Regensburg, 93053 Regensburg, Germany
[§]Department of Chemistry, Lomonosov Moscow State University, 119991 Moscow, Russia
[⊥]Kurnakov Institute of General and Inorganic Chemistry RAS, 119991 Moscow, Russia

Supporting Information

ABSTRACT: Four new transition metal-free pnictide representatives of the LaOAgS structure type were predicted by DFT calculations and found in the BaFMgPn (Pn = P, As, Sb and Bi) family. The compounds adopt the tetragonal space group *P4/nmm* with the unit cell parameters *a*/*c* 4.3097(1) Å/9.5032(1) Å, 4.3855(1) Å/9.5918(1) Å, 4.5733(1) Å/9.8184(1) Å, and 4.6359(1) Å/9.8599(1) Å, respectively. According to the DFT calculations, these new compounds are semiconductors with band gaps steadily decreasing from Pn = P (*ca.* 2 eV) to Pn = Bi (*ca.* 1 eV). The corresponding strontium fluoride and rare-earth oxide analogs are unlikely to exist and have not been observed yet. The trends of the stability within 1111 and structurally and/or chemically related compounds based on a combined consideration of geometry and DFT calculations are discussed.

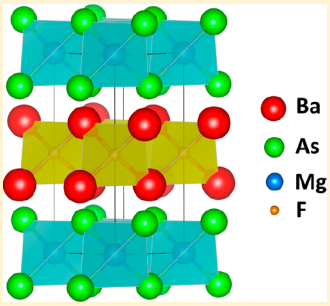

INTRODUCTION

The discovery of a new unconventional class of superconducting materials, the iron-based pnictide superconductors, in 2008[1,2] has renewed attention to compounds involving 2D antifluorite structural fragments, which can be termed layered antifluorites. Among the latter, two particularly widespread structure types have received the greatest attention, the $ThCr_2Si_2$ structure type (termed "122")[3] with the highest known number of representatives (exceeding 1000 by now),[4] and the LaOAgS structure type[5] where the highest superconducting transition temperature was observed.[6] The latter is sometimes distinguished from the related ZrCuSiAs structure type.[7] Both are generally summarized as "1111" (Figure 1) despite exhibiting different bonding schemes.[8] Besides superconductivity, the LaOAgS type comprises representatives exhibiting many other intriguing properties, e.g., Ag^+-based ionic conductivity of the archetype,[5] optical transparency vs. electric conductivity in doped Cu and Ag chalcogenides,[9] colossal magnetoresistance (CMR) in doped Mn pnictides,[10] or thermoelectricity in doped LaOZnSb.[11] The considerably high number of representatives (approaching 300[12,13]) can be explained by the relatively simple atomic arrangement best described as alternation of two very common motifs, the *type-anti-type* related fluorite (litharge, PbO) and antifluorite (mackinawite, FeS) type slabs (Figure 1). Based on the chemical composition of the litharge part, its representatives can be separated into several groups. Most numerous are oxide compounds containing $[M_2O_2]^{n+}$ (M = Th, U−Pu for n = 4, and Bi, La−Er for n = 2) slabs;[14−17] fluorides containing $[M'_2F_2]^{2+}$ fragments (M′ = Ca, Sr, Ba, or Eu[18−26]) are less common mostly due to the smaller variety of the divalent cations; hydrides are the rarest,[27] and there exists only one unique nitrogen-based compound, $ThN_{1-x}O_xFeAs$.[28]

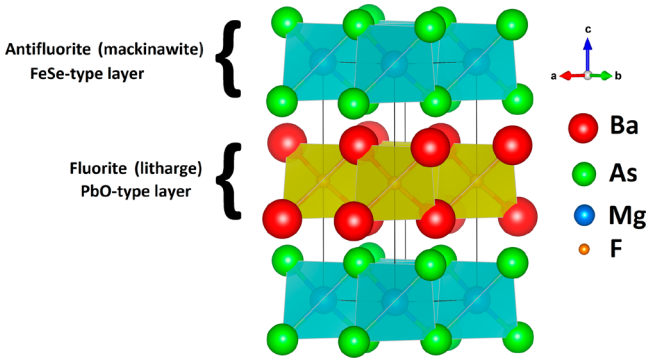

Figure 1. Crystal structure of BaFMgAs—a new representative of the 1111 family—comprising fluorite- and antifluorite-type layers of $[Ba_2F_2]^{2+}$ and $[Mg_2As_2]^{2-}$, respectively.

We note that the chemistry of PbO and FeSe slabs observed separately in related structures is essentially more diverse,[17] and the number of their possible combinations into 1111 can be estimated as high as *ca.* 800, e.g., just below the number of known $ThCr_2Si_2$-type compounds. The factors restricting their actual number are charge-balance, and chemical (mostly redox) and geometrical compatibility of the constituting layers. However, several groups of suggested combinations which seem not to violate any of the criteria listed above remain as

Received: December 20, 2018
Published: February 21, 2019

DOI: 10.1021/acs.inorgchem.8b03554
Inorg. Chem. 2019, 58, 3435−3443

Table 1. Details of the PXRD experiments for BaFMgPn (Pn = P, As, Sb, Bi)

compound	BaFMgP	BaFMgAs	BaFMgSb	BaFMgBi
phase composition	target phase +4.7(1)% BaF_2	target phase +2.5(1)% BaF_2	target phase +3.5(1)% BaF_2	single phase
space group		*P*4/*nmm* (origin choice 2)		
cell parameters[a]				
a, Å	4.3097(1)	4.3855(1)	4.5733(1)	4.6359(1)
c, Å	9.5032(1)	9.5918(1)	9.8184(1)	9.8599(1)
V, Å^3	176.51(1)	184.48(1)	205.35(1)	211.91(1)
density, g/cm^3	3.982	4.6	4.89	6.106
radiation		Mo Kα_1		
2θ range, deg	3−55	2−55	3−63	3−63
data points	3467	3543	4082	4082
overall params	38	36	34	34
reflections	153	159	243	261
struct params	8	10	9	9
R values				
R_F	1.6	2.3	2.31	2.96
R_P	4.82	3.2	4.45	1.43
R_{wP}	6.64	4.38	6.58	1.93
χ^2	1.79	1.99	3.56	1.5

[a]In order to obtain more realistic standard deviations all the provided values should be multiplied by a factor of 3.

yet unaddressed. Since most of the properties listed above are associated with mackinawite-type layers involving transition metals, the compounds of pre- and post-transition elements received very little attention. Thus, a detailed knowledge on their existence is necessary for elucidation and exact formulation of compatibility criteria and selection rules to predict which new representatives are likely and unlikely to exist before undertaking the synthesis which commonly requires complicated synthetic procedures or expensive precursors. Our prediction and successful synthesis of two transition metal-free tetrelides, BaFAlSi and BaFAlGe,[19] prompted us at investigation of some other valence isoelectronic systems, the most likely representatives being compounds involving $[Mg_2Pn_2]^{2-}$ (Pn = P−Bi) slabs observed in a series of ternary CeFeSi-type group 1−group 2 pnictides. We also note that the Mg−Pn distances in structurally characterized NaMgAs, NaMnSb[29] and KMgPn (Pn = P, As, Sb, and Bi)[30] are rather close to the Cd−Pn ones observed in BaFCdPn,[21,26] suggesting the existence of BaFMgPn compounds. The relatively large size of the mackinawite-type slabs makes the $[Ba_2F_2]^{2+}$ litharge-type slabs the best candidates for their counterparts; as in the previous cases, possible Sr−F and Ln−O analogs were also considered.

EXPERIMENTAL SECTION

Synthesis and Primary Characterization. The starting compounds were elemental Mg, Ca, Sr, Ba, La, P, As, Sn, and Bi (purity >99%), as well as SrF_2, BaF_2, and MgO (the latter calcined at 600 °C overnight before use). New compounds were attempted via a high-temperature solid state route using La + MgO + Pn starting mixtures in ∼1:1:1 or Ba (Sr) + BaF_2 (SrF_2) + Mg + Pn in ∼1:1:2:2 ratios. All operations were performed in an Ar-filled glovebox (M'Braun). The barium compounds were prepared in the following way: metallic barium (Sigma-Aldrich, 99.5%) was chopped in the glovebox right prior to the preparation; powdered BaF_2 (Chempur, 99.999%) was dried at 373 K before use; cuttings of metallic Mg (99.5%) as well as red phosphorus (Chempur, > 99%), arsenic (Chempur, 99.9%), antimony (Chempur, 99.99%) and bismuth (purity) were used as purchased. The starting materials were mixed according to the 1111 composition (using 5−10% excess of Ba metal, 2−3% excess of BaF_2 and 2% excess of Mg), and then loaded in graphite crucibles which were flame-sealed in evacuated silica tubes. The samples were annealed for 48−72 h at 1223, 1173, 1073, and 973 K (2 K/min heating rate) for BaFMgP, BaFMgAs, BaFMgSb, and BaFMgBi, respectively. Intermediate products were homogenized with 2% excess of Mg metal, and annealed according to the same protocol for another 100 h. The as-prepared samples are extremely oxygen and moisture sensitive black powders which decompose in air to mixtures of oxides (hydroxides) and fluorides within minutes. They also readily react with water and acids releasing flammable gases. This behavior reminds one of that of the tetrelides BaFAlTt (Tt = Si, Ge), which are however essentially more stable in dry air or in contact with pure water.[19]

Powder Diffraction Patterns. Powder diffraction patterns for phase analysis as well as high-quality data sets for structure refinements were collected on a STOE STADI P diffractometer (Mo Kα_1 radiation, λ = 0.70930 Å, Ge (111) monochromator, Dectris MYTHEN 1K detector). The powdered samples were loaded in quartz capillaries of 0.3 mm diameter and spun during the measurements. The temperature was controlled at 293 K during the measurement. The WinXPOW software package from STOE &Ciewas was used for data collection and processing.[31] Four new BaFMgPn compounds were found to be present in the samples as majority phases. In all other cases, no signs of the target compounds were observed.

Elemental Composition. Elemental composition was confirmed using a Zeiss EVO MA 15 scanning electron microscope equipped with a Bruker Quantax EDX system with an X Flash Detector 630 M. Traces of oxygen were found to be present due to partial decomposition.

Structure Refinement. Since no single-crystals of the target phases could be produced during the synthesis crystal structures were refined from high-resolution (d_{min} < 0.8 Å) X-ray powder diffraction data sets using the Rietveld method, implemented in the JANA2006 software package.[32] The crystal structures of previously reported analogs were used as starting models. A standard mathematical apparatus for the description of the peak profile (Pseudo-Voigt profile function, Legendre polynomials for background) was used. The refinements proceeded in a straightforward manner. The relatively strong absorption of X-rays was corrected according to the model for Debye−Scherrer geometry to achieve realistic values of atomic displacement parameters. Further details of the powder diffraction experiments are collected in Table 1, refined atomic coordinates and displacement parameters are summarized in Table 2; selected interatomic distances are listed in Table 3, and the final Rietveld refinement plots are shown in Figure 2. A projection of the BaFMgAs unit cell (Figure 1) is drawn by the VESTA software.[33]

DOI: 10.1021/acs.inorgchem.8b03554
Inorg. Chem. 2019, 58, 3435−3443

Table 2. Atomic Coordinates and Displacement Parameters (in Å^2)

atom	position	*x/a*	*y/b*	*z/c*	U_{iso}
			BaFMgP		
Ba1	2*c*	1/4	1/4	0.15982(7)	0.0112(2)
P1	2*c*	1/4	1/4	0.6532(3)	0.0099(6)
Mg1	2*b*	1/4	3/4	1/2	0.0138(9)
F1	2*a*	1/4	3/4	0	0.010(1)
			BaFMgAs		
Ba1	2*c*	1/4	1/4	0.1547(1)	0.0201(3)
As1	2*c*	1/4	1/4	0.6610(2)	0.0193(5)
Mg1	2*b*	1/4	3/4	1/2	0.019(2)
F	2*a*	1/4	3/4	0	0.021(3)
			BaFMgSb		
Ba1	2*c*	1/4	1/4	0.14046(8)	0.0172(2)
Sb1	2*c*	1/4	1/4	0.67501(9)	0.0161(3)
Mg1	2*b*	1/4	3/4	1/2	0.007(1)
F1	2*a*	1/4	3/4	0	0.020(2)
			BaFMgBi		
Ba1	2*c*	1/4	1/4	0.1363(1)	0.0165(5)
Bi1	2*c*	1/4	1/4	0.6819(1)	0.0137(3)
Mg1	2*b*	1/4	3/4	1/2	0.012(2)
F1	2*a*	1/4	3/4	0	0.018(4)

Thermal Behavior. Thermal behavior was studied via differential thermal analysis (DTA) utilizing a SETARAM TG-DTA 92 analyzer. The samples were loaded in silica capillaries and subjected to 2 heating and cooling cycles. No obvious thermal effects are observed up to 1273K. However, container deterioration was observed, which suggests gradual release of magnesium vapor at elevated temperatures.

DFT Calculations. Electronic structure calculations were performed at the density functional theory (DFT) level using two approaches: (i) the all-electron full-potential linearized augmented plane wave method (FP-LAPW) as implemented in the ELK code,[34] and (ii) the pseudopotential projector augmented wave method (PAW) as implemented in the Vienna *ab initio* simulation package (VASP).[35,36]

In the first approach, which was used for energy calculations, the Perdew−Burke−Enzerhoff exchange-correlation functional revised for solids (PBESol) of the GGA-type was utilized.[37] The Brillouin zone sampling was performed using a 7 × 7 × 3 *k*-point grid, the muffin-tin sphere radii r_{MT} for the respective atoms were (Bohr): 2.80 (Ba, Bi), 2.60 (Sb), 2.40 (As), 2.20 (Mg, P), 2.00 (F), and the maximum moduli for the reciprocal vectors k_{max} were chosen so that $r_{MT}k_{max}$= 9.0.

In the second approach, which was used for both energy calculations and unit cell optimization, a Monckhorst−Pack[38] *k*-point mesh of 14 × 14 × 6 was employed, and the energy cutoff was set at 500 eV. The PBESol exchange-correlation functional of the GGA-type and SCAN exchange-correlation functional of the meta-GGA-type,[39] augmented with a nonlocal correlation part from the rVV10 van der Waals density functional, were used in the PAW-based calculations. The latter was used to take the potentially layered nature of the compounds into account, which would imply dispersive interactions between the layers. Unit cell optimization for the hypothetical LaOMgPn (Pn = P, As, Sb and Bi) compounds and for SrFMgAs was performed using the PBESol functional. Starting models were taken from the respective barium−magnesium fluoropnictides. Unit cell metrics, its symmetry, and atomic coordinates were allowed to relax in each case. The convergence criterion for forces in ionic relaxation was set to 0.001 eV/Å.

Atomic charges were calculated in accordance with R. Bader's quantum theory of atoms in molecules (QTAIM)[40] using the DGrid4.6 package[41] and Bader code,[42−44] utilizing ELK wave functions or VASP charge density, respectively, as inputs. The estimations of structure stabilities were made according to the approach established in ref 26 by comparing calculated total energies of quaternary compounds and their precursors. The electron localization function (ELF)[45] was calculated by the internal VASP routine.

RESULTS AND DISCUSSION

Synthesis. Compared to the previously reported cases,[22−24,26] the synthesis of BaFMgPn type compounds is more complex due to high reactivity and volatility of magnesium above its melting point (~920 K) and extreme air and moisture sensitivity of the target products. Although no thermal effects were observed for all four compounds up to 1273K, the synthesis temperature had to be decreased when passing from BaFMgP (1223K) to BaFMgBi (973 K). This can be explained assuming lower reactivity of magnesium toward heavier pnictogens and competitive reactions of Ba and Mg vapors with the walls of the silica ampules. The effects of the latter can be suppressed by introducing a slight (~2%) excess of metallic Mg and Ba; adding a slight excess of BaF_2 also favors the formation of the target compounds against ternary $BaMg_2Pn_2$[46] compounds. Similar attempts to prepare LaOMgAs led to samples mostly consisting of MgO along with some poorly crystalline phases; annealed samples with nominal composition SrFMgAs consist mostly of SrF_2 and $SrMg_2As_2$ along with binary strontium and magnesium arsenides.

Crystal Structures. As noted before, the structures of the new compounds represent regular commensurate sequences of $[Ba_2F_2]^{2+}$ (litharge-type) and $[Mg_2Pn_2]^{2-}$ (mackinawite-type) layers represented in Figure 1. These are formed by condensation (via edge sharing) of tetragonally ($\bar{4}3m \rightarrow \bar{4}2m$) distorted FBa_4 and $MgPn_4$ tetrahedra which flatten or stretch along the $\bar{4}$ axis to provide the commensurate overall structure. This results in splitting of six initially equal edges into groups of 2 (unshared, equal to the *a* cell parameter, corresponding angle α_2) and 4 (shared, α_4); the same is observed for the bond angles while the four center-to-vertex distances (corresponding to the Ba−F and Mg−Pn bonds) remain equal. The deviation of the bond angles from the ideal

Table 3. Selected interatomic distances (in Å) and angles (in deg.; defined in results and discussion section)

	BaFMgP	BaFMgAs	BaFMgSb	BaFMgBi
d(Ba−F)	2.6363(4)	2.6476(8)	2.6703(4)	2.6792(5)
d(Mg−Pn)	2.601(2)	2.682(2)	2.8603(5)	2.9308(6)
d(Ba−Pn)	3.528(2)	3.570(1)	3.7068(6)	3.7362(7)
d(Mg−Mg)	3.04740(4)	3.1010(1)	3.2338(1)	3.2781(1)
α_2(Ba−F−Ba)	109.65(1)	111.83(1)	117.81(1)	119.80(1)
α_4(Ba−F−Ba)	109.39(1)	108.31(1)	105.47(1)	104.57(1)
α_2(Pn−Mg−Pn)	111.91(1)	109.71(1)	106.15(1)	104.53(1)
α_4(Pn−Mg−Pn)	108.29(1)	109.35(1)	111.16(1)	112.00(1)

DOI: 10.1021/acs.inorgchem.8b03554
Inorg. Chem. 2019, 58, 3435−3443

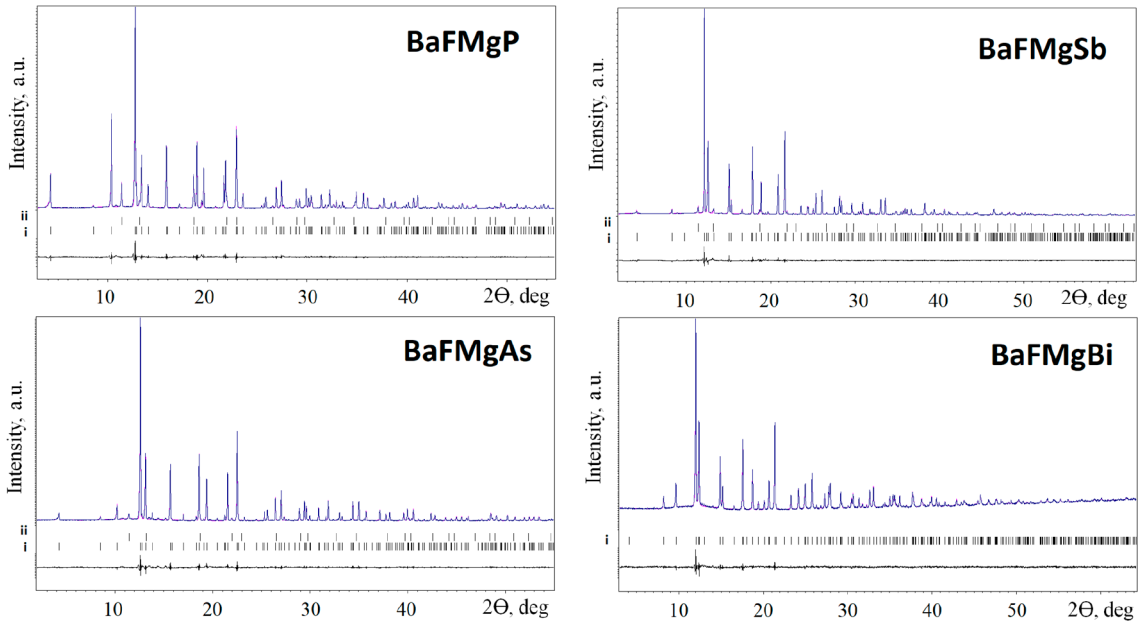

Figure 2. Experimental (blue), calculated (magenta), and difference plots (the Rietveld refinement plots) for BaFMgPn (Pn = P, As, Sb and Bi) series. The reflections of the main phases are marked as **i**, traces of BaF_2 impurities are marked as **ii.**.

angle of 109.5° and the differences between them reflect the degree of the distortion.

As follows from Table 3 and illustrated in Figure 3, BaFMgP features almost regular FBa_4 tetrahedra, while the MgP_4 moieties are slightly flattened. Following the trend in atomic radii, the next representative, BaFMgAs, exhibits a longer distance d(Mg−Pn), which results in a slight flattening of the FBa_4 tetrahedra while the $MgAs_4$ counterparts are now almost regular. The heavier analogs, BaFMgSb and BaFMgBi, are characterized by increasingly flattened FBa_4 but elongated $MgSb_4$ and $MgBi_4$ tetrahedra since d(Mg−Pn) > d(Ba−F). The same trend is observed in the crystal structures of other BaFTPn (T = Zn, Mn, and Cd) compounds.[26] The values of α_2 and α_4 of 119.8° and 104.6° in BaFMgBi are very close to those observed in the structure of BaFI;[47] however, they are probably rather close to the tolerance limit for the distortion of the FBa_4 tetrahedra. The BaFMgBi bismuthide exhibits the hitherto largest values of the a parameter and the cell volume among all 1111 type compounds. As in the isostructural series, along with the angular distortions of the tetrahedra, the distances d(Ba−F) elongate from 2.636 to 2.679 Å. The layered nature of BaFMgPn implies that the atoms forming the interface between the layers, Ba and Pn, have asymmetric coordination, i.e., they are surrounded by four F (Mg) at short distances (2.6−2.9 Å) from inside of the layer and by four Pn (Ba) at longer distances (3.5−3.7 Å) from the opposite side, as shown in Figure 4.

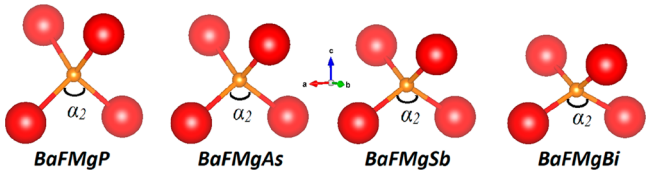

Figure 3. Evolution of FBa_4 tetrahedra in the BaFMgPn series (Pn = P, As, Sb, and Bi). The angle α_2 increases when passing to heavier pnictides, thus flattening the tetrahedra FBa_4. F atoms are yellow; Ba atoms are red. The distances between atoms are not drawn to the scale.

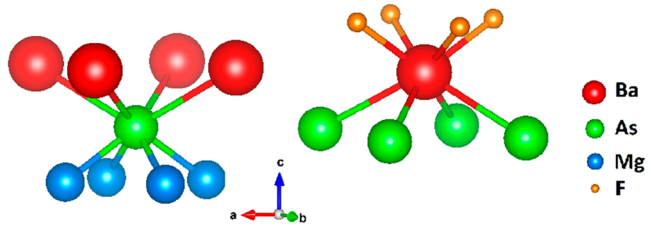

Figure 4. First coordination spheres of Ba and As in the structure of BaFMgAs.

The unit cell metrics for the new compounds as well as for the related groups of BaFMnPn, BaFZnPn and BaFCdPn are compared in Table 4. The unit cell parameters and volumes for BaFMgPn are comparable to those of BaFCdPn and slightly higher than for BaFZnPn and BaFMnPn. The c/a ratio, being slightly smaller than for BaFMnPn and BaFZnPn, also classifies BaFMgPn into the same group as BaFCdPn. The decreased c/a ratio implies a tendency for $MgPn_4$ and $CdPn_4$ tetrahedra to be more flattened along the 4-fold axis as compared to $MnPn_4$ and $ZnPn_4$, and thus, to dictate a higher a unit cell parameter. This in turn dictates the $[Mg_2Pn_2]^{2-}$ layer to be stretched, so that the intergrowths can exist only with the biggest fluorite layers like $[Ba_2F_2]^{2+}$. The expected distortions for the smaller $[Sr_2F_2]^{2+}$ and $[La_2O_2]^{2+}$ layers seem to be too large. Hence the desired intergrowths with $[Mg_2Pn_2]^{2-}$ counterparts were not observed experimentally, in agreement with the results of DFT calculations (*see below*).

Electronic Structure, Stability, and Bonding Analysis. Total (TDOS) and projected (PDOS) densities of states near the Fermi level for BaFMgPn (Pn = P, As, Sb and Bi) are shown in Figure 5. According to the calculations, all these compounds are semiconductors, with band gaps decreasing from Pn = P to Pn = Bi. All methods used (FP-LAPW/PBESol,

DOI: 10.1021/acs.inorgchem.8b03554
Inorg. Chem. 2019, 58, 3435−3443

Table 4. Unit Cell Parameters for the Compounds BaFTPn (T = Mg, Zn, Mn, Cd)

		BaFMgPn	BaFZnPn	BaFMnPn	BaFCdPn
Pn = P	*a*, Å	4.3097(1)	4.1563(1)	4.1793(2)	4.3300(1)
	c, Å	9.5032(1)	9.4574(3)	9.5040(5)	9.4933(2)
	c/*a*	2.205	2.275	2.274	2.192
	V, Å^3	176.51(1)	163.38(1)	166.00(2)	177.99(1)
Pn = As	*a*, Å	4.3855(1)	4.2383(1)	4.2739(1)	4.4008(1)
	c, Å	9.5918(1)	9.5260(2)	9.5875(2)	9.5466(2)
	c/*a*	2.187	2.247	2.243	2.169
	V, Å^3	184.48(1)	171.12(1)	175.13(1)	184.89(1)
Pn = Sb	*a*, Å	4.5733(1)	4.4384(2)	4.4791(1)	4.5792(9)[a]
	c, Å	9.8184(1)	9.7789(6)	9.8297(2)	9.740(4)[a]
	c/*a*	2.147	2.203	2.195	2.127
	V, Å^3	205.35(1)	192.64(2)	197.21(1)	204.24(9)[a]
Pn = Bi	*a*, Å	4.6359(1)		4.5384(1)	
	c, Å	9.8599(1)		9.8929(2)	
	c/*a*	2.127		2.18	
	V, Å^3	211.91(1)		203.76(1)	

[a]Single-crystal data reported at 200 K[21]

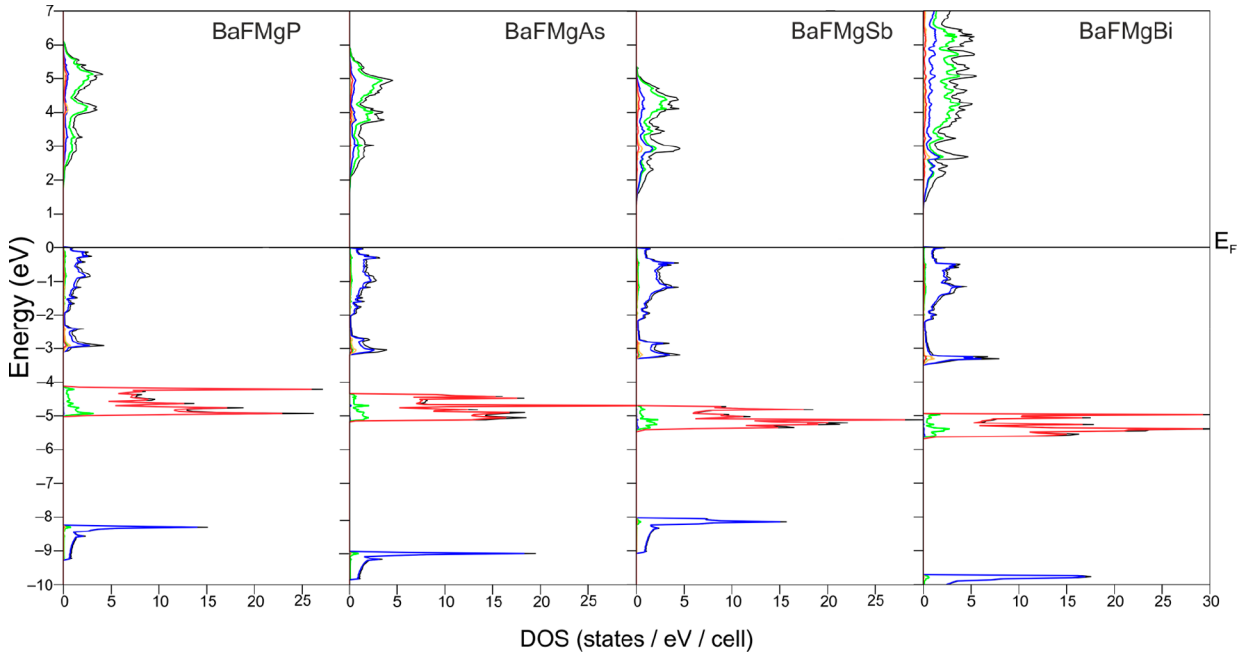

Figure 5. Total (TDOS) and projected (PDOS) densities of states for BaFMgPn (Pn = P−Bi) calculated from VASP/PBESol data: TDOS, black line; Ba PDOS, green line; Pn PDOS, blue line; Mg PDOS, yellow line; F PDOS, red line.

PAW/PBESol, PAW/SCAN) show this effect consistently, although numerical values of the calculated band gaps differ somewhat. For FP-LAPW/PBESol, they are 1.69 (BaFMgP), 1.50 (BaFMgAs), 1.16 (BaFMgSb), and 0.96 eV (BaFMgBi). For VASP calculations that utilize PBESol we obtain bang gaps of 1.75 (BaFMgP), 1.58 (BaFMgAs), 1.25 (BaFMgSb), and 1.04 eV (BaFMgBi), while the respective band gaps calculated from SCAN-based results are *ca.* 0.4−0.5 eV wider. On the one hand, DFT is known to often underestimate band gaps of semiconductors, and thus wider gaps predicted by the more advanced SCAN functional could be at first glance considered an improvement. On the other hand, the results from PBESol-based calculations by both all-electron and pseudopotential approaches not only agree well with each other but also are in much better agreement with the fact that all four compounds are black. Thus, in this particular case, while both PBESol and SCAN produce qualitatively the same picture, the results obtained with the former are closer to the observed properties of the compounds. We have attempted to measure diffuse reflectance spectra for all compounds to obtain an experimental band gap values. Unfortunately, most of the data turned out to be unusable due to the severe air-instability of BaFMgPn. Probably the only spectrum that was possible to interpret was obtained in the case of BaFMgBi (see Figure S1 in the Supporting Information), which shows the band gap in BiFMgBi to be *ca.* 0.9 eV, which is in good agreement with calculated values.

In all four compounds, the top of the valence band is essentially formed by the *p*-states of pnictogen atoms (see Figure 5), while the bottom of the conduction band features strong contribution from barium *s*-states, along with smaller for Pn = P, but increasing from P to Bi to the extent of being

DOI: 10.1021/acs.inorgchem.8b03554
Inorg. Chem. 2019, 58, 3435−3443

almost equal, contribution from pnictogen *p*-states, and even smaller contribution from fluorine *p*-states and magnesium *s*-states. The zoomed DOS around the Fermi level for BaFMgPn is given in Figure S2 in the Supporting Information. Thus, the band gap in this series is mostly formed by barium and pnictogen atoms, which is somewhat different from the previously investigated series of Ba and Eu d-metal fluoropnictides[23,24,26] where the cations in the fluorine-containing block provided relatively smaller contributions to the states in vicinity of the Fermi level. This reflects the key difference between the series of AFTPn compounds, where A = Sr, Ba, and Eu and T = transition metal, and the BaFMgPn series under discussion, namely the change of the chemical nature of the metal in the metal−pnictogen block. With the change from *d*-metal to *s*-metal, the contributions near the Fermi level from the metal in the M−Pn block become comparable to the contribution from the metal in the M−F block.

Calculated QTAIM charges for the BaFMgPn series are shown in Table 5. There is a very significant charge density transfer from barium and magnesium to fluorine and the pnictogens, making all structures essentially ionic. Barium and magnesium charges are the same in BaFMgP and slightly diverge upon going toward Pn = Bi as the pnictogen atom electronegativity gradually decreases, resulting in a slightly decreasing positive charge on magnesium. Nevertheless, effective atomic charges are still high and indicate a predominantly ionic nature even for BaFMgBi, which is expected to have the least ionicity in the magnesium−pnictogen structure blocks across the whole series. This might help to rationalize the results obtained with the SCAN functional, as the main idea behind its use here was to account for potential dispersion interactions, while the interatomic interactions turned out to be mostly of Coulomb type. Thus, it is possible that the highly ionic bonding nature of these compounds nullifies the benefits from using more advanced functionals in this case. Additional support to the ionic nature of bonding in these compounds is provided by the lack of nonatomic attractors in the topology of the electron localization function (ELF), even in the case of BaFMgBi (see Figure 6).

Table 5. Calculated Atomic Charges for BaFMgPn (Pn = P, As, Sb, and Bi) from ELK/Dgrid (E) and VASP/Bader (V) Data

Compound	Ba	F	Mg	Pn
BaFMgP (E)	+1.52	−0.84	+1.53	−2.21
BaFMgP (V)	+1.52	−0.83	+1.52	−2.21
BaFMgAs (E)	+1.52	−0.85	+1.51	−2.18
BaFMgAs (V)	+1.52	−0.84	+1.48	−2.16
BaFMgSb (E)	+1.51	−0.86	+1.47	−2.12
BaFMgSb (V)	+1.51	−0.85	+1.44	−2.10
BaFMgBi (E)	+1.50	−0.86	+1.42	−2.05
BaFMgBi (V)	+1.49	−0.86	+1.38	−2.01

The results of the investigation of the thermodynamic stabilities of BaFMgPn, LaOMgPn and SrFMgAs based on specific reactions are summarized in Tables 6 and 7. All BaFMgPn compounds are found to be stable with respect to their likely precursors, with free enthalpies of the respective reactions (estimated at 0 K where entropy contribution is zero) being in the range of *ca.* −15 to −20 kJ/mol. This agrees with our observations during the syntheses, confirming that the compounds do not need to be quenched to avoid decomposition, and the main handling problem is their high reactivity rather than intrinsic instability. On the contrary,

Table 6. Optimized Structural Parameters of Hypothetical LaOMgPn and SrFMgAs According to DFT/VASP Calculations (Tetragonal, *P4/nmm*)

	LaOMgP	LaOMgAs	LaOMgSb	LaOMgBi	SrFMgAs
a, Å	4.1219	4.1723	4.3071	4.3409	4.2111
c, Å	8.9002	9.0821	9.5120	9.7466	9.0268
z (La)[a]	0.1315	0.1265	0.1134	0.1096	0.1443
z (Pn)[a]	0.6721	0.6800	0.6940	0.6977	0.6790

[a]Atomic coordinate ($^1/_4$; $^1/_4$; *z*).

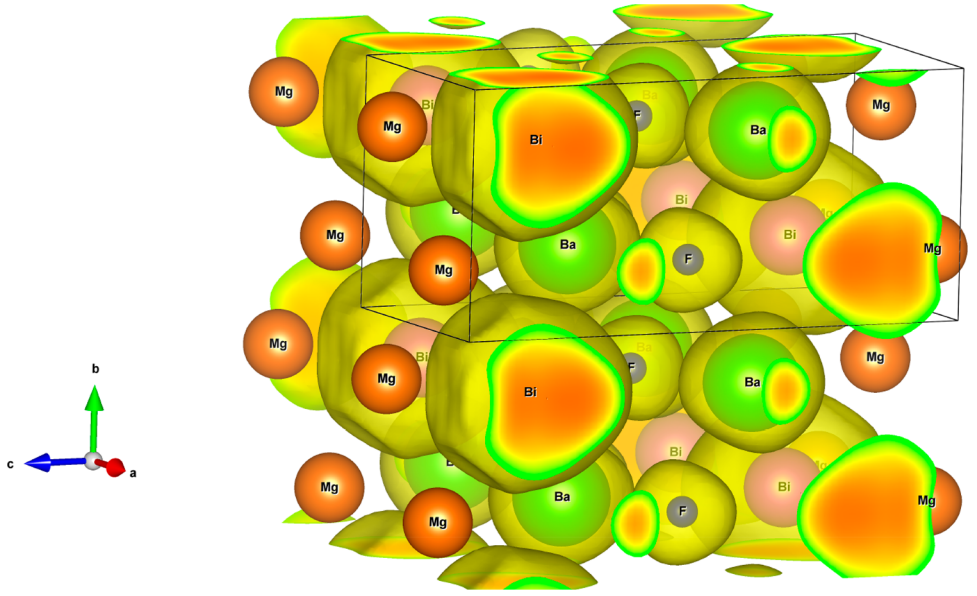

Figure 6. ELF isosurface (η = 0.53) for BaFMgBi calculated from the VASP data.

DOI: 10.1021/acs.inorgchem.8b03554
Inorg. Chem. 2019, 58, 3435−3443

Table 7. Energy Gain and Free Enthalpies of BaFMgPn, SrFMgAs, and LaOMgPn (Pn = P, As, Sb, and Bi) Formation According to Specific Reactions

	Pn = P		Pn = As		Pn = Sb		Pn = Bi	
Reaction	-ΔE, eV	ΔG, kJ/mol	ΔE, eV	ΔG, kJ/mol	ΔE, eV	ΔG, kJ/mol	ΔE, eV	ΔG, kJ/mol
1[a]	0.155	**−15**	0.187	**−18.1**	0.208	**−20.1**	0.223	**−21.5**
2[b]	–	–	−0.025	2.4	–	–	–	–
3[c]	−0.405	39.1	−0.381	36.8	−0.501	48.3	−0.395	38.1

[a]1, BaF_2 + $BaMg_2Pn_2$ = 2BaFMgPn [b]2, SrF_2 + $SrMg_2As_2$= 2SrFMgAs (estimations for a hypothetical compound) [c]3, LaPn + MgO = LaOMgPn (estimations for hypothetical compounds)

optimized structures of hypothetical oxygen-containing analogs of fluoropnictides (the LaOMgPn series), as well as the strontium analogue of BaFMgAs, are found to be unstable with respect to their precursors (LaPn + MgO or SrF_2 + $SrMg_2As_2$, respectively). This explains why our synthetic attempts to produce these compounds were not successful. SrFMgAs has significantly less positive free enthalpy as compared to the LaOMgPn series. Nevertheless, it is still deemed unfavorable, which agrees with the experimental observations. The compound was chosen since, in our experience and from the literature,[25] arsenides of this structure type are always found even in the cases when the corresponding phosphide and/or antimonide analogs do not exist. The same probably applies to other SrFMgPn compounds which are as unlike to exist (no synthetic attempts and calculations were made). The general pattern is the same as for the AeFCdPn compounds[21,26] which is not surprising given the Mg−Pn distances being very close to Cd−Pn. It has to be noted that these predictions are only relevant to the 1111-type structures and reaction pathways specified in this paper; yet, our synthetic experience shows that when the target phase is not obtained, the precursors/decomposition products, AeF_2 + AeT_2Pn_2, in the respective reactions properly reflect phase compositions of the samples.

The new compound BaFMgBi is the second bismuthide representative of the 1111 structure type, the first being BaFMnBi.[20] Though the estimated distortions of the TBi_4 tetrahedra in the hypothetical compounds BaFZnBi and BaFCdBi should be of the same order like those in BaFMgBi, all our attempts to prepare these compounds have not yet been successful.[26] In the meantime, such mackinawite-type slabs have been observed in the structures of intermetallic compounds (Sr,Ba)TBi_2.[48,49] The reason is likely the same as we had suggested for nonexistence of valence isoelectronic compounds BaFAlSn and BaFGaTt (Tt = tetrel). In these cases, the mackinawite-type layers are expected to exhibit the largest degree of bond covalence while combinations of layers with essentially different bond nature (ionic/covalent or ionic/metallic) seem to be unfavorable. Evidently, studies in chemically related systems are necessary to verify our suggestions. Another interesting point is that the structures of our compounds contain two IIA group metals playing essentially different crystallographic roles. Similar patterns are observed in the structures of the CeFeSi-type compounds BaMgTt[50] due to the very large size difference of Ba^{2+} and Mg^{2+}.[51]

CONCLUSION

Using solid state techniques, we successfully prepared a chemically novel family of 1111-type layered fluoropnictides via introducing a second nontransitional metal, magnesium, into the antifluorite part of the structure. According to DFT calculations, these compounds are semiconductors with calculated band gaps decreasing from *ca.* 2 eV (Pn = P) to *ca.* 1 eV (Pn = Bi). Bonding analysis shows predominantly ionic nature of chemical bonds in both Ba−F and Mg−Pn parts of the structures. Despite the fact that the compounds feature magnesium in the role more conventionally played by *p*- or *d*-block metals, main crystallographic features of this series fit the trends observed for the other members of the family, e.g., gradual band gap decrease with increasing Pn atomic number, very well. The same holds for the trends in geometrical parameters of their crystal structures which are similar to the families of group 11 (Cu, Ag), 12 (Zn, Cd), and Mn-containing compounds.

This series, on the one hand, is a good example to show the flexibility of the LaOAgS structure type and to display its further perspectives with regard to even more exotic elemental compositions. On the other hand, very good agreement between theoretical predictions and experimental efforts in these systems encourages further use of theory in the search for new representatives of this structure type, as well as some closely related compounds.

ASSOCIATED CONTENT

Supporting Information

The Supporting Information is available free of charge on the ACS Publications website at DOI: 10.1021/acs.inorgchem.8b03554.

Diffuse reflectance spectrum for BaFMgBi and calculated total and projected DOS of the region around the Fermi level for BaFMgPn (PDF)

Accession Codes

CCDC 1881369, 1881375, 1881383, and 1881391 contain the supplementary crystallographic data for this paper. These data can be obtained free of charge via www.ccdc.cam.ac.uk/data_request/cif, or by emailing data_request@ccdc.cam.ac.uk, or by contacting The Cambridge Crystallographic Data Centre, 12 Union Road, Cambridge CB2 1EZ, UK; fax: +44 1223 336033.

AUTHOR INFORMATION

Corresponding Authors

*E-mail: igor.plohih@gmail.com (I.V.P.).
*E-mail arno.pfitzner@ur.de (A.P.).

ORCID

Igor V. Plokhikh: 0000-0003-1638-2771
Andrei V. Shevelkov: 0000-0002-8316-3280
Arno Pfitzner: 0000-0001-8653-7439

Author Contributions

The manuscript was written through contributions of all authors. All authors have given approval to the final version of the manuscript.

DOI: 10.1021/acs.inorgchem.8b03554
Inorg. Chem. 2019, 58, 3435−3443

Notes

The authors declare no competing financial interest.

■ ACKNOWLEDGMENTS

We thank the Russian Foundation for Basic Researches for the support of this study under Grant No. 16-03-00661a. I.V.P. thanks BAYHOST and the DAAD. A.N.K. acknowledges the support from the Russian Science Foundation (Grant No. 14-13-01115) and the use of shared facilities of the Lomonosov MSU Supercomputer Center.

■ REFERENCES

(1) Kamihara, Y.; Hiramatsu, H.; Hirano, M.; Kawamura, R.; Yanagi, H.; Kamiya, T.; Hosono, H. Iron-based layered superconductor: LaOFeP. *J. Am. Chem. Soc.* **2006**, *128*, 10012.

(2) Kamihara, Y.; Watanabe, T.; Hirano, M.; Hosono, H. Iron-based layered superconductor $La[O_{1-x}F_x]FeAs$ (x = 0.05−0.12) with T_C = 26K. *J. Am. Chem. Soc.* **2008**, *130*, 3296.

(3) Ban, Z.; Sikirica, M. The crystal structure of ternary silicides ThM_2Si_2 (M= Cr, Mn, Fe, Co, Ni and Cu). *Acta Crystallogr.* **1965**, *18*, 594.

(4) Just, G.; Paufler, P. On the coordination of $ThCr_2Si_2$ ($BaAl_4$-type compounds within the field of free parameters. *J. Alloys Compd.* **1996**, *232*, 1.

(5) Palazzi, M.; Carcaly, C.; Flahaut, J. Un nouveau conducteur ionique (LaO)AgS. *J. Solid State Chem.* **1980**, *35*, 150.

(6) Ishida, K.; Nakai, Y.; Hosono, H. To what extent iron-pnictide new superconductors have been clarified: a progress report. *J. Phys. Soc. Jpn.* **2009**, *78*, 062001.

(7) Johnson, V.; Jeitschko, W. ZrCuSiAs: a "filled" PbFCl type. *J. Solid State Chem.* **1974**, *11*, 161.

(8) Charkin, D. O.; Zolotova, X. N. A crystallographic re-investigation of Cu_2Sb-related binary, ternary, and quaternary structures: how many structure types can exist upon the same topology of a unit cell? *Crystallogr. Rev.* **2007**, *13*, 201.

(9) Ueda, K.; Hiramatsu, H.; Hirano, M.; Kamiya, T.; Hosono, H. Wide-gap layered oxychalcogenide semiconductors: Materials, electronic structures and optoelectronic properties. *Thin Solid Films* **2006**, *496*, 8.

(10) Wildman, E. J.; Mclaughlin, A. C. A variable temperature synchrotron X-ray diffraction study of colossal magnetoresistant $NdMnAsO_{0.95}F_{0.05}$. *Sci. Rep.* **2016**, *6*, 20705.

(11) Suzuki, T.; Bahramy, M. S.; Arita, R.; Taguchi, Y.; Tokura, Y. Doping control and thermoelectric properties in $R_{1-x}A_xZnSbO$ (R = La, Ce; A = Ca, Sr). *Phys. Rev. B: Condens. Matter Mater. Phys.* **2011**, *83*, 035204.

(12) Pöttgen, R.; Johrendt, D. Materials with ZrCuSiAs-type structure. *Z. Naturforsch., B: J. Chem. Sci.* **2008**, *63*, 1135.

(13) Johrendt, D.; Pöttgen, R. Pnictide oxides: a new class of high T_C superconductors. *Angew. Chem., Int. Ed.* **2008**, *47*, 4782.

(14) Kusainova, A. M.; Berdonosov, P. S.; Akselrud, L. G.; Kholodkovskaya, L. N.; Dolgikh, V. A.; Popovkin, B. A. New layered compounds with the general composition (MO)(CuSe), where M = Bi, Nd, Gd, Dy, and BiOCuS: syntheses and crystal structure. *J. Solid State Chem.* **1994**, *112*, 189.

(15) Muir, S.; Subramanian, M. A. ZrCuSiAs type layered oxypnictides: A bird's eye view of LnMPnO compositions. *Prog. Solid State Chem.* **2012**, *40*, 41.

(16) Park, S. W.; Mizoguchi, H.; Kodama, K.; Shamoto, S. I.; Otomo, T.; Matsuishi, S.; Hosono, H.; et al. Magnetic Structure and Electromagnetic Properties of LnCrAsO with a ZrCuSiAs-type Structure (Ln = La, Ce, Pr, and Nd). *Inorg. Chem.* **2013**, *52*, 13363.

(17) Clarke, S. J.; Adamson, P.; Herkelrath, S. J. C.; Rutt, O. J.; Parker, D. R.; Pitcher, M. J.; Smura, C. F. Structures, physical properties, and chemistry of layered oxychalcogenides and oxypnictides. *Inorg. Chem.* **2008**, *47*, 8473.

(18) Kabbour, H.; Cario, L.; Boucher, F. Rational design of new inorganic compounds with the ZrSiCuAs structure type using 2D building blocks. *J. Mater. Chem.* **2005**, *15*, 3525.

(19) Charkin, D. O.; Plokhikh, I. V.; Kuznetsov, A. N.; Kazakov, S. M. BaFAlSi and BaFAlGe: First transition metal-free LaOAgS-type fluoride tetrelides. *J. Alloys Compd.* **2015**, *627*, 451.

(20) Saparov, B.; Singh, D. J.; Garlea, V. O.; Sefat, A. S. Crystal, magnetic, and electronic structures, and properties of new BaMnPnF (Pn = As, Sb, Bi). *Sci. Rep.* **2013**, *3*, 2154.

(21) Saparov, B.; Bobev, S. Synthesis, crystal and electronic structures of the new quaternary phases $A_5Cd_2Sb_5F$ (A = Sr, Ba, Eu), and $Ba_5Cd_2Sb_5O_x$ (0.5 < x< 0.7). *Dalton Trans.* **2010**, *39*, 11335.

(22) Charkin, D. O.; Urmanov, A. V.; Kazakov, S. M. Preparation and crystal structures of novel LaOAgS-type copper and silver fluoride chalcogenides. *J. Alloys Compd.* **2012**, *516*, 134.

(23) Plokhikh, I. V.; Charkin, D. O.; Verchenko, V. Yu.; Kuznetsov, A. N.; Kazakov, S. M.; Tsirlin, A. A.; Shevelkov, A. V. Structural and thermodynamic stability of the "1111"structure type: a case study of the EuFZnPn series. *Inorg. Chem.* **2016**, *55*, 12409.

(24) Plokhikh, I. V.; Charkin, D. O.; Verchenko, V. Yu.; Kuznetsov, A. N.; Kazakov, S. M.; Tsirlin, A. A.; Shevelkov, A. V. Synthesis, crystal structure and physical properties of europium − manganese fluoride pnictides, EuMnPnF (Pn = P, As, Sb). *J. Solid State Chem.* **2018**, *258*, 682.

(25) Zhu, X.; Han, F.; Cheng, P.; Mu, G.; Shen, B.; Fang, L.; Wen, H.-H. Superconductivity in fluoride-arsenide $Sr_{1-x}La_xFeAsF$ compounds. *Europhys. Lett.* **2009**, *85*, 17011.

(26) Charkin, D. O.; Urmanov, A. V.; Plokhikh, I. V.; Korshunov, A. D.; Kuznetsov, A. N.; Kazakov, S. M. Synthesis and crystal structures of novel LaOAgS-type alkaline earth − zinc, manganese, and cadmium fluoride pnictides. *J. Alloys Compd.* **2014**, *585*, 644.

(27) Tencé, S.; Matar, S. F.; André, G.; Gaudin, E.; Chevalier, B. Hydrogenation inducing ferromagnetism in the ternary antiferromagnet NdCoSi. *Inorg. Chem.* **2010**, *49*, 4836.

(28) Wang, C.; Wang, Z.-C.; Mei, Y.-X.; Li, Y.-K.; Li, L.; Tang, Z.-T.; Liu, Y.; Zhang, P.; Zhai, H.-F.; Xu, Z.-A.; Cao, G.-H. A new ZrCuSiAs-type superconductor: ThFeAsN. *J. Am. Chem. Soc.* **2016**, *138*, 2170.

(29) Krenkel, B.; Schuster, H.-U. NaMgAs(Sb) - ternary compounds in a modified Cu_2Sb structure. *Z. Naturforsch., B: J. Chem. Sci.* **1978**, *33*, 1080.

(30) Vogel, R.; Schuster, H.-U. Neue elektrovalente ternäre Verbindungen des Kaliums mit Magnesium und Elementen der 5. Hauptgruppe. *Z. Naturforsch., B: J. Chem. Sci.* **1979**, *34b*, 1719.

(31) *STOE WinXPOW*, Version 3.10, STOE &Cie GmbH: Darmstadt, Germany, 2016.

(32) Petricek, V.; Dusek, M.; Palatinus, L. Crystallographic computing system JANA2006: general features. *Z. Kristallogr. - Cryst. Mater.* **2014**, *229*, 345.

(33) Momma, K.; Izumi, F. VESTA 3 for three-dimensional visualization of crystal, volumetric and morphology data. *J. Appl. Crystallogr.* **2011**, *44*, 1272.

(34) *ELK, an all-electron full-potential linearized augmented-plane wave (FP-LAPW) code*, ver. 3.1.12; http://elk.sourceforge.net.

(35) Kresse, G.; Joubert, D. From ultrasoft pseudopotentials to the projector augmented-wave method. *Phys. Rev. B: Condens. Matter Mater. Phys.* **1999**, *59*, 1758.

(36) Kresse, G.; Furthmüller, J. *Vienna Ab-initio Simulation Package (VASP)*, v.5.4.4; http://vasp.at.

(37) Perdew, J. P.; Ruzsinszky, A.; Csonka, G. I.; Vydrov, O. A.; Scuseria, G. E.; Constantin, L. A.; Zhou, X.; Burke, K. Restoring the density-gradient expansion for exchange in solids and surfaces. *Phys. Rev. Lett.* **2008**, *100*, 136406.

(38) Monkhorst, H. J.; Pack, J. D. Special points for Brillouin-zone integrations. *Phys. Rev. B* **1976**, *13*, 5188.

(39) Peng, H.; Yang, Z.-H.; Perdew, J. P.; Sun, J. Versatile van der Waals density functional based on a meta-generalized gradient approximation. *Phys. Rev. X* **2016**, *6*, 041005.

DOI: 10.1021/acs.inorgchem.8b03554
Inorg. Chem. 2019, 58, 3435−3443

(40) Bader, R. F. W. *Atoms in Molecules: A Quantum Theory*. Oxford University Press: Oxford, U.K., 1990.
(41) Kohout, M. *DGrid, ver. 4.6*; Radebeul: 2011.
(42) Henkelman, G.; Arnaldsson, A.; Jónsson, H. A fast and robust algorithm for Bader decomposition of charge density. *Comput. Mater. Sci.* **2006**, *36*, 354.
(43) Sanville, E.; Kenny, S. D.; Smith, R.; Henkelman, G. An improved grid-based algorithm for Bader charge allocation. *J. Comput. Chem.* **2007**, *28*, 899.
(44) Yu, M.; Trinkle, D. R. Accurate and efficient algorithm for Bader charge integration. *J. Chem. Phys.* **2011**, *134*, 064111.
(45) Silvi, B.; Savin, A. Classification of chemical bonds based on topological analysis of electron localization functions. *Nature* **1994**, *371*, 683.
(46) Klüfers, P.; Mewis, A. AB_2X_2-Verbindungen mit $CaAl_2Si_2$-Struktur. X. Zur Struktur neuer ternärer Erdalkaliphosphide und –arsenide. *Z. Kristallogr.* **1984**, *169*, 135.
(47) Liebich, B. W.; Nicollin, D. Refinement of the PbFCl types BaFI, BaFBr and CaFCl. *Acta Crystallogr., Sect. B: Struct. Crystallogr. Cryst. Chem.* **1977**, *33*, 2790.
(48) Cordier, G.; Eisenmann, B.; Schäfer, H. Darstellung und Kristallstruktur von $SrCu_2Sb_2$ und $SrZnBi_2$. *Z. Anorg. Allg. Chem.* **1976**, *426*, 205.
(49) Brechtel, E.; Cordier, G.; Schäfer, H. Neue ternäre Erdalkali-Übergangselement-Pnictide. *J. Less-Common Met.* **1981**, *79*, 131.
(50) Eisenmann, B.; Schäfer, H.; Weiss, A. Der Übergang vom ″geordneten″ Anti-$PbCl_2$-Gitter zum anti-PbFCl-Gitter: ternäre Phasen ABX der Erdalkalimetalle mit Elementen der 4. Hauptgruppe (A = Ca, Sr, Ba; B = Mg; X = Si, Ge, Sn, Pb). *Z. Anorg. Allg. Chem.* **1972**, *391*, 241.
(51) Shannon, R. D. Revised effective ionic radii and systematic studies of interatomic distances in halides and chalcogenides. *Acta Crystallogr., Sect. A: Cryst. Phys., Diffr., Theor. Gen. Crystallogr.* **1976**, *A32*, 751.

DOI: 10.1021/acs.inorgchem.8b03554
Inorg. Chem. 2019, 58, 3435−3443